Radiological Physics and Technology (2023) 16:195–202
https://doi.org/10.1007/s12194-023-00706-5

RESEARCH ARTICLE

Impact of bone-equivalent solution density in a thoracic spine phantom on bone single-photon emission computed tomography image quality and quantification

Norikazu Matsutomo[1] · Mitsuha Fukami[1] · Tomoaki Yamamoto[1]

Received: 25 November 2022 / Revised: 13 February 2023 / Accepted: 14 February 2023 / Published online: 6 March 2023

Abstract
This study aimed to evaluate the effects of dipotassium hydrogen phosphate (K_2HPO_4) solution density on single-photon emission computed tomography (SPECT) image quality and quantification. We used a JSP phantom containing six cylinders filled with K_2HPO_4 solutions of varying densities. Computed tomography (CT) was performed, and CT values and linear attenuation coefficients were measured. Subsequently, SPECT images of an SIM^2 bone phantom filled with ^{99m}Tc with/without K_2HPO_4 solution were acquired using a SPECT/CT camera. The full width at half maximum (FWHM), percentage coefficient of variation (%CV), recovery coefficient, and standardized uptake value (SUV) were evaluated to investigate the impact of the K_2HPO_4 solution density. The CT values and linear attenuation coefficients increased with the K_2HPO_4 solution density. The CT values for cancellous and cortical bones were reflected by K_2HPO_4 solution densities of 0.15–0.20 and 1.50–1.70 g/cm^3, respectively. FWHM values were significantly lower with the K_2HPO_4 solution than those with water alone (18.0 ± 0.9 mm with water alone, 15.6 ± 0.2 mm with 0.15 g/cm^3 K_2HPO_4, and 16.1 ± 0.3 mm with 1.49 g/cm^3 K_2HPO_4). Although the %CVs showed no significant differences, the recovery coefficients obtained with water alone tended to be slightly lower than those obtained with the K_2HPO_4 solution. The SUV obtained using the standard density of the K_2HPO_4 solution differed from that obtained using the optimized density. In conclusion, SPECT image quality and quantification depends on the presence and concentration of the bone-equivalent solution. The optimal bone-equivalent solution density should be used to evaluate the bone image phantoms.

Keywords Bone scintigraphy · Dipotassium hydrogen phosphate · Phantom · Single-photon emission computed tomography · Positron emission tomography

1 Introduction

Single-photon emission computed tomography (SPECT) helps diagnose and evaluate various bone diseases and metastases found on bone scintigraphy [1–4]. However, bone SPECT image quality and quantification are strongly affected by acquisition conditions, reconstruction parameters, and several image corrections [5, 6]. Therefore, several studies using commercially available thoracic spine phantoms, such as the SIM^2 bone phantom, have been performed to evaluate this novel technology, provide new evidence, and improve consistency in practice [7–9].

The SIM^2 bone phantom (Kyoto Kagaku Co., Ltd., Kyoto, Japan) was developed by Ichikawa et al. to evaluate bone SPECT image quality and quantification accuracy [10]. It simulates the thorax, including the spine, tumor, mediastinum, and lungs. It consists of a dipotassium hydrogen phosphate (K_2HPO_4) solution with ^{99m}Tc to mimic the vertebrae, tumors of the spine, and spinous and transverse processes. K_2HPO_4 is a bone-equivalent solution with a composition comparable to that of cranium [11]. In most cases, the K_2HPO_4 solution is prepared by dissolving 100 g of K_2HPO_4 in 67 g of distilled water [12, 13]. However, the human body

✉ Norikazu Matsutomo
nmatsutomo@ks.kyorin-u.ac.jp

Mitsuha Fukami
mitsuha-f@ks.kyorin-u.ac.jp

Tomoaki Yamamoto
tyamamoto@ks.kyorin-u.ac.jp

[1] Department of Medical Radiological Technology, Faculty of Health Sciences, Kyorin University, B-524, 5-4-1 Shimorenjaku Mitaka-shi, Tokyo 181-8612, Japan

has two types of bone tissue: cortical and trabecular. The vertebrae are primarily trabecular bones. CT yields highly variable Hounsfield unit (HU) values, ranging from 300 to 3000 (trabecular bone, approximately 300 HU; cortical bone, approximately 1200 HU), for bone tissue [14]. In CT attenuation correction (CTAC), linear attenuation maps are generated to use the HU values that are converted to attenuation coefficients to correct the emission data for photon attenuation. HUs are defined by the physical density of the tissues and the atomic number of the constituent elements. They are proportional to the absorption/attenuation of photon energy. Therefore, the density of the bone-equivalent solution should be optimal to reflect the targeted bone tissues in phantom studies, particularly when CTAC is being used. Although the accuracy of K_2HPO_4 solution has been evaluated using a ^{153}Gd transmission line source[11], its optimal density for a specific bone phantom has not been validated in CTAC.

This study aimed to validate the effect of K_2HPO_4 solution density on SPECT image quality and quantification, and to determine the optimal K_2HPO_4 solution density for CTAC using the SIM^2 bone phantom. We evaluated the relationship between K_2HPO_4 solution density and HU values on CT images and determined the effects of differences in the filling solution of the phantom spine on image quality and quantification.

2 Materials and methods

2.1 SPECT/CT instrument and phantoms

All experimental data were acquired using a dual-head SPECT/CT camera (Infinia 8Hawkeye 4; GE Healthcare, Chicago, IL, USA) equipped with a low-energy, high-resolution collimator. This system had 2.54-cm (1″) thick crystals and a spatial resolution of 8.1 mm with ^{99m}Tc at a distance of 10 cm from the collimator. The CT component was a low-dose, four-slice, slow-rotation X-ray CT system. Standard clinical scan parameters were as follows: tube voltage, 140 kV; tube current, 2.5 mA; slice thickness, 5 mm; CT reconstruction kernel, standard, and helical scan. To optimize the K_2HPO_4 solution density, we used a cylindrical phantom (JSP type; Kyoto Kagaku Co., Ltd., Kyoto, Japan) containing six fillable cylinders (Fig. 1a). In addition, the SIM^2 bone phantom filled with ^{99m}Tc was used to evaluate the effect of K_2HPO_4 solution density on ^{99m}Tc activity and linear attenuation distribution functions (Fig. 1b, c). This phantom consisted of four parts: a trunk (background), cylinder (vertebra), four spheres of different sizes (tumors), and T-shaped container (transverse and spinous processes). The axis and height of the trunk were 290 and 300 mm, respectively. The diameters of the four tumor-simulating spheres were 13, 17, 22, and 28 mm.

2.2 K_2HPO_4 solution density

The optimal K_2HPO_4 solution density was assessed using a JSP phantom consisting of six fillable cylinders. The cylinders were filled with a K_2HPO_4 solution with densities ranging from 0.10 to 1.85 g/cm^3. The inclusion density was experimentally determined based on the solubility of K_2HPO_4 in water (167 g/100 mL). As only six cylinders were available, the measurements were performed in two batches. The background area was filled with water. Subsequently, a CT scan was performed using standard clinical scan parameters. Six circular regions of interest with 25-mm diameters were placed on the object part, and the mean CT values and linear attenuation coefficients were measured on CT images and correction maps, respectively (Fig. 2).

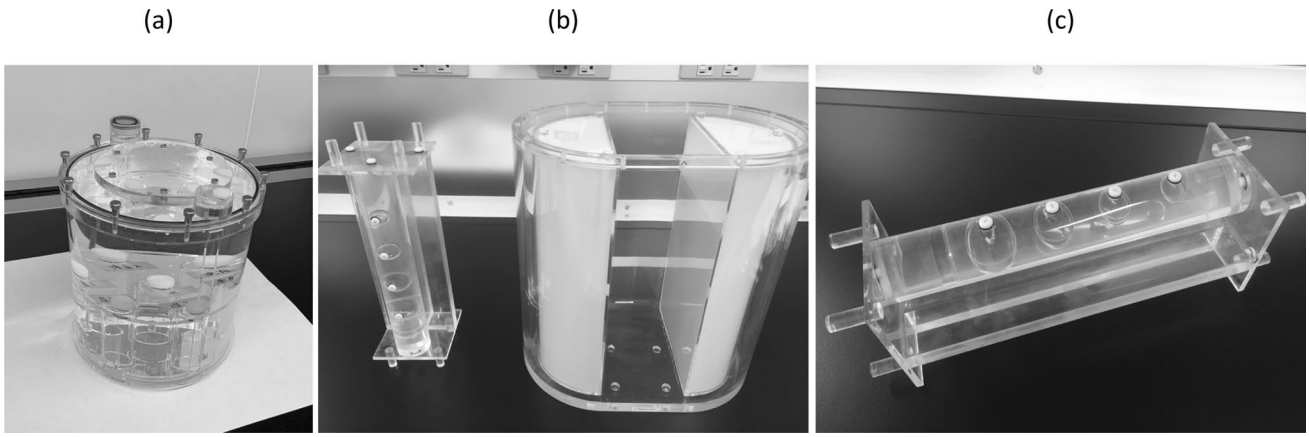

Fig. 1 Photograph of each phantom. **a** Cylindrical phantom with six cylinders. **b** Overview of the SIM^2 bone phantom. **c** The spine comprises the vertebra, tumors, and transverse and spinous processes

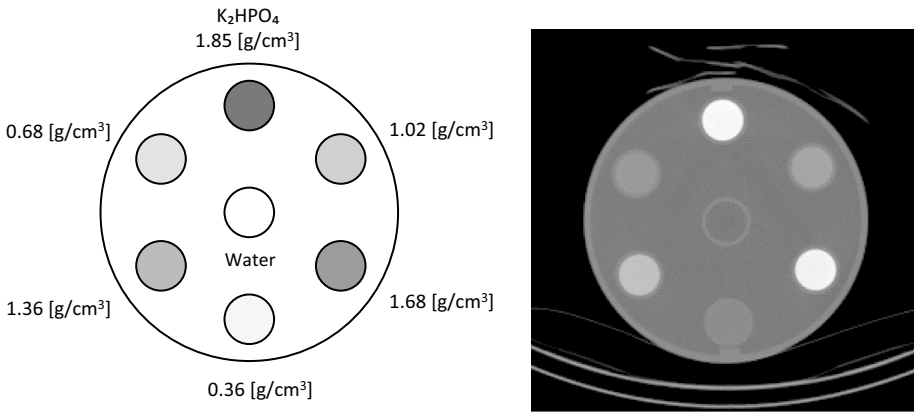

Fig. 2 The phantom contains six cylinders with different K_2HPO_2 densities. Right: CT image

Table 1 Radioactivity concentration of each part of the SIM^2 bone phantom

		Water	K_2HPO_4	
			Optimized density 0.15 g/cm^3	Standard density 1.49 g/cm^3
kBq/mL	BG	9.4	6.5	6.8
	Vertebra	72.4	64.0	63.6
	Tumor	490.0	340.0	350.0
	TB ratio	52.1	52.3	51.5

TB tumor-to-background, *K_2HPO_4* dipotassium hydrogen phosphate

2.3 Impact of the bone-equivalent liquid condition

2.3.1 SIM^2 bone phantom

We created a SIM^2 bone phantom using three patterns (Table 1). The vertebra and tumor parts on the SIM^2 bone phantom were filled with ^{99m}Tc in water or K_2HPO_4 solution at a concentration of 0.15 (optimized density) or 1.49 g/cm^3 (standard density). The concentrations were determined as described in the previous section. The background was filled with 9.4, 6.5, and 6.8 kBq/mL of ^{99m}Tc. The tumor-to-background ratio was set to approximately 50.

2.3.2 Image acquisition and reconstruction

All the SIM^2 bone phantom data were acquired using a dual-head SPECT/CT camera with a low-energy high-resolution collimator. The projection data were obtained thrice in repeated continuous mode at 5 min/rotation × three times (total acquisition time: 30 min). The matrix number was 128 × 128 and the step angle was 3°. The main energy and scatter windows were set to 140.0 keV ± 10% and 120.0 keV ± 5%, respectively. The distance from the collimator to the phantom was 230 mm. The CT scan parameters were as follows: slice thickness, 6.1 mm; slice spacing, 4.42 mm; matrix, 512 × 512; voltage, 140 kV; current, 2.5 mA; CT reconstruction kernel, standard and helical pitch, 1.9. All SPECT images were reconstructed using ordered-subset expectation maximization with resolution recovery correction, dual-energy window scatter correction, and CTAC. The reconstruction parameters were 10 subsets and 5 iterations. The images were reconstructed by post-processing with a Butterworth filter (cutoff frequency, 0.4 cycles/cm; power factor, 10).

2.4 Data analysis

The spatial resolution and percent coefficient of variation (%CV), recovery coefficients, and standardized uptake value (SUV) were calculated to investigate the impact of K_2HPO_4 solution density (Fig. 3). The spatial resolution was evaluated using the full width at half maximum (FWHM) of the spinous process. Horizontal profiles were plotted on the spinous processes of the reconstructed images for the five slices, and the FWHM was calculated accordingly. In addition, we placed a 36 × 36 × 36-mm cylindrical volume of interest (VOI) on the trunk (background) of the phantom. The %CVs of the background were calculated as follows:

$$\%CV = \frac{SD_b}{C_b} \times 100\%$$

where C_b is the mean count in the background VOI and SD_b is the standard deviation of the background area based on the variance in individual voxels within the VOI.

For the recovery coefficients and SUV, cylindrical and circular VOIs were placed on the vertebral and tumor parts, respectively. The recovery coefficients and mean SUVs (SUV_{mean}) were calculated as follows.

$$RC = \frac{C_{\text{tumor}}}{C_{\text{reference}}}$$

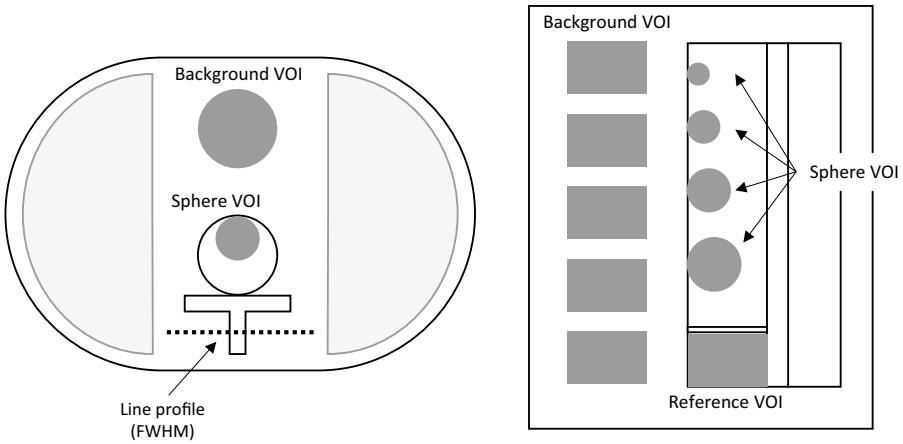

Fig. 3 Setting of the volume of interest and line profile for evaluation

$$\mathrm{SUV} = \frac{\mathrm{SPECT\,counts/Calibration\,factor}}{\mathrm{Injected\,activity/Phantom\,weight}}$$

where C_{tumor} is the mean count in the VOIs of the tumor parts and $C_{reference}$ is the reference VOI count for the vertebral part. The SUV_{mean} values of the tumor and background were calculated using GI-BONE software (AZE Co., Ltd., Tokyo, Japan). The calibration factor was obtained automatically from the correlation between radioactivity and counts per second of a cylinder phantom in each iteration using the GI-BONE software. The FWHM, %CV, and SUV_{mean} of the background were compared using the Tukey–Kramer method. Differences were considered statistically significant at p values < 0.05.

3 Results

3.1 Mean CT values and linear attenuation coefficients

Figure 4 shows the mean CT values and linear attenuation coefficients of the K_2HPO_4 solution density. The CT values increased with an increasing K_2HPO_4 solution density and tended to decrease the changes in CT values over 1.5 g/cm^3. The CT values for cancellous and cortical bones were reproduced by K_2HPO_4 solution densities of 0.15–0.20 and 1.50–1.70 g/cm^3, respectively. Similarly, the linear

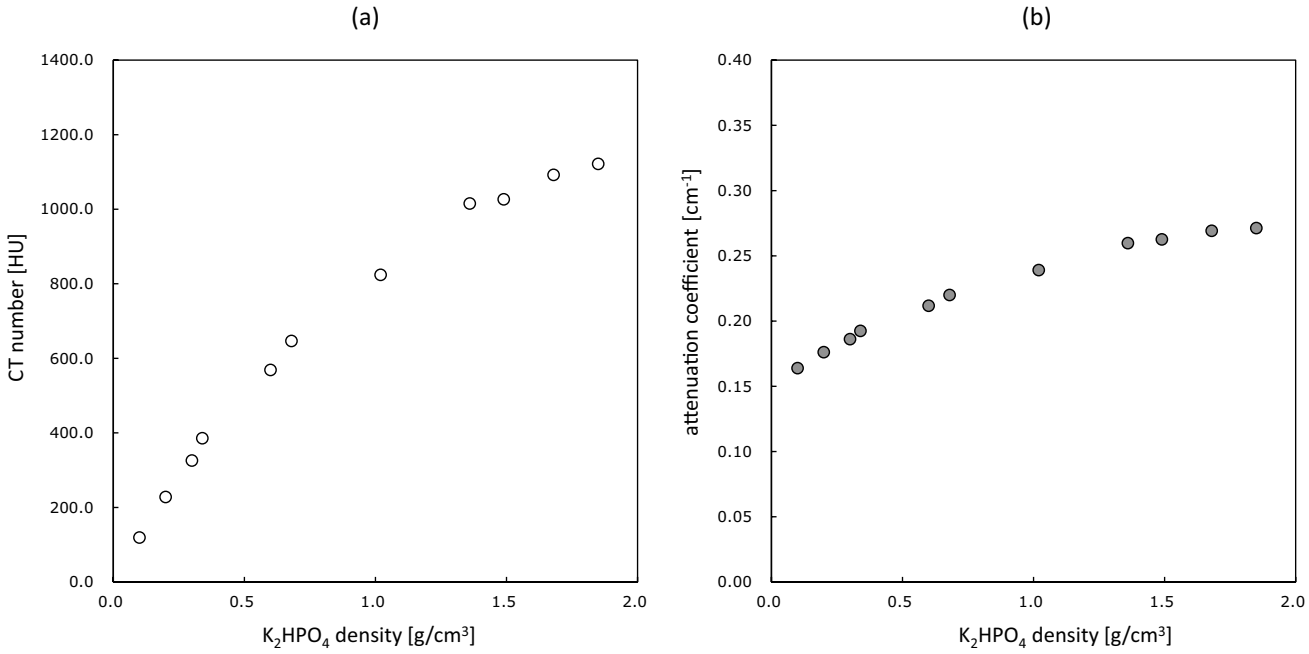

Fig. 4 CT values (**a**) and linear attenuation coefficients (**b**). The CT values and linear attenuation coefficients increased with the K_2HPO_4 solution density. The CT values for the cancellous bone were reflected by a K_2HPO_4 solution density of 0.15–0.20 g/cm^3

attenuation coefficient slowly increased with increasing K_2HPO_4 solution density.

3.2 FWHM, %CV, and recovery coefficient

Figure 5 shows the FWHM and %CV values for the SIM^2 bone phantom obtained for each K_2HPO_4 solution density and with water alone. The FWHM values were significantly lower with K_2HPO_4 solution than those with water alone (Fig. 5a):18.0 ± 0.9 mm for water alone, 15.6 ± 0.2 mm for 0.15 g/cm^3 K_2HPO_4, and 16.1 ± 0.3 mm for 1.49 g/cm^3 K_2HPO_4. The background %CVs (Fig. 5b) showed no significant difference. Figure 6 shows the recovery coefficients obtained for each phantom condition. The recovery coefficients did not differ significantly between 0.15 and 1.49 g/cm^3 K_2HPO_4. However, the recovery coefficients tended to be slightly lower with water alone than those with K_2HPO_4 solution.

3.3 SUV_{mean}

Figure 7 shows the SUV_{mean} of each sphere and the background. The result of the K_2HPO_4 solution was different from the result of the water alone for all sphere sizes. In addition, the SUV_{mean} obtained using the standard density of the K_2HPO_4 solution differed from that obtained using the optimized density (0.15 g/cm^3). Figure 8 shows the representative CT and SPECT images. Although the accumulation values of background areas were not the same, the visibility of the vertebral bodies and spinous processes depended on the presence/absence and concentration of the bone-equivalent solution.

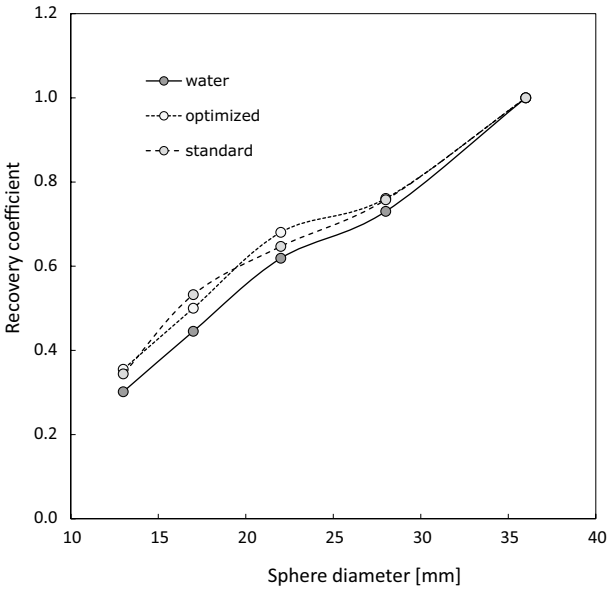

Fig. 6 Correlation between the recovery coefficient and K_2HPO_4 solution density. The recovery coefficients showed different patterns depending on whether a K_2HPO_4 solution or water was used

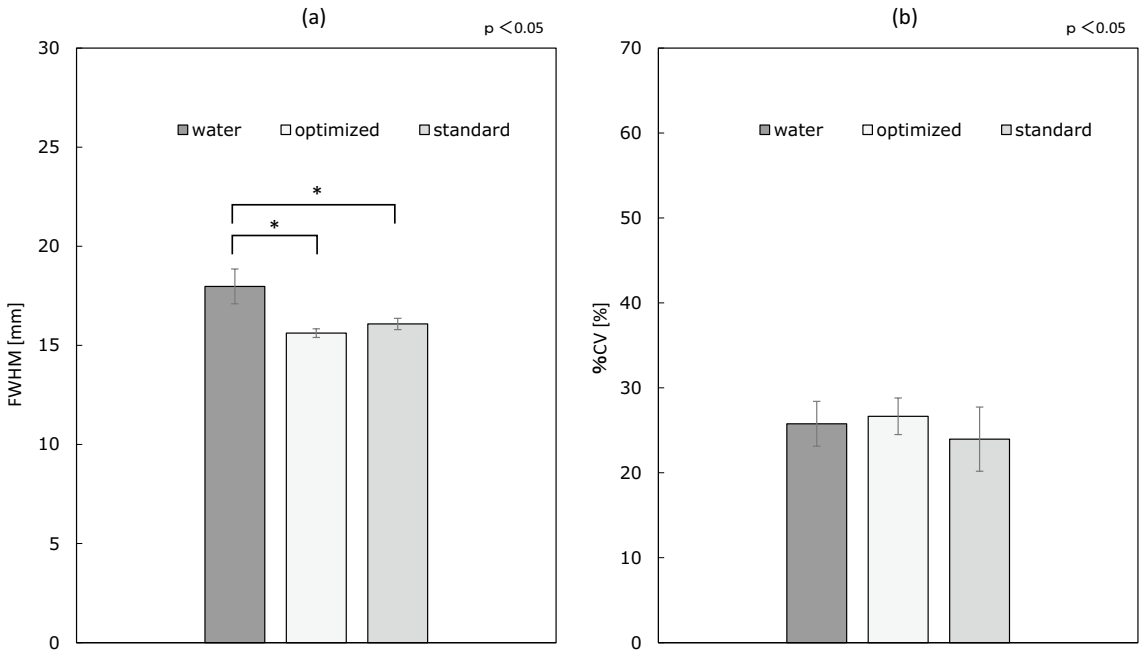

Fig. 5 Graphs showing the FWHM (**a**) and %CV (**b**). Although the %CV did not change with the phantom condition, the FWHM values with the K_2HPO_4 solution were significantly decreased compared to those with water alone

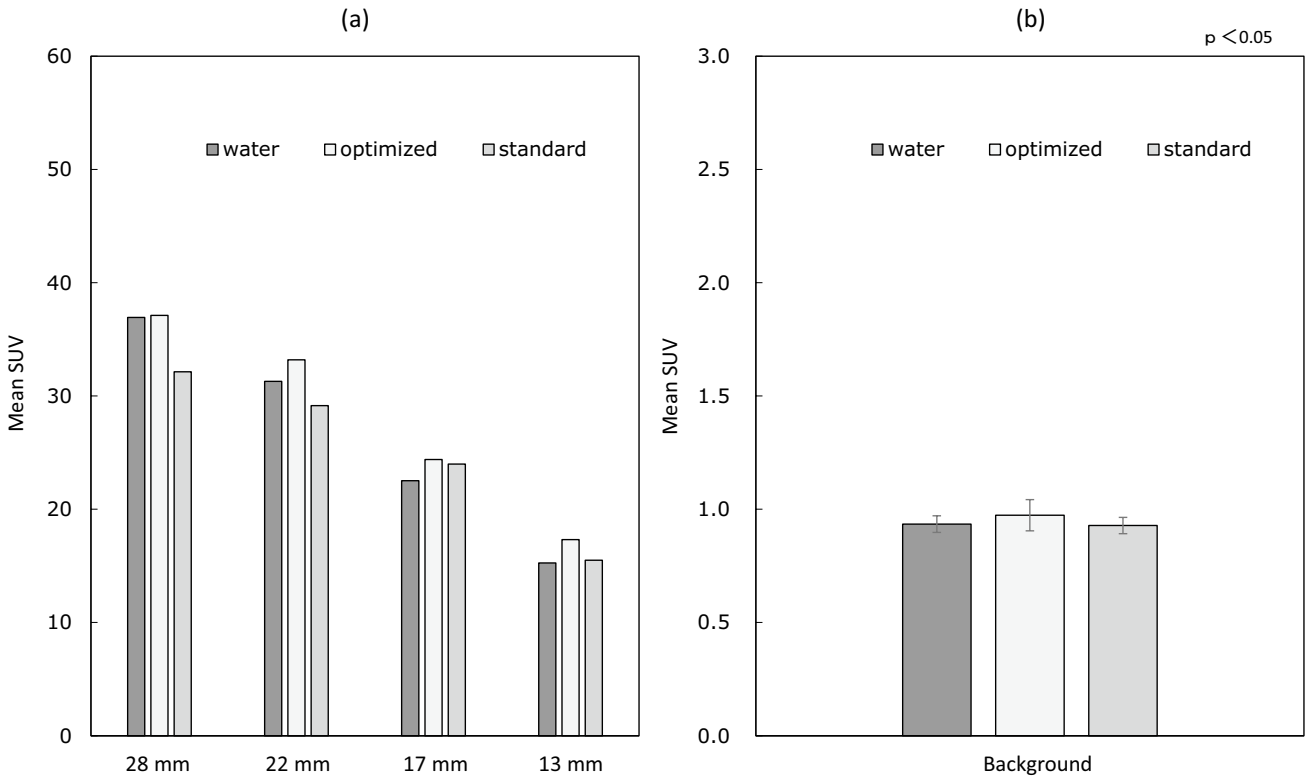

Fig. 7 SUV_{mean} according to the sphere (**a**) and background (**b**). Sphere SUV_{mean} differed significantly between the K_2HPO_4 solution and water. However, the SUV_{mean} in the background did not change under the phantom condition

4 Discussion

In this study, we evaluated the SPECT/CT imaging of SIM^2 bone phantoms containing a bone-equivalent solution comprising K_2HPO_4 at different concentrations and the effect of K_2HPO_4 concentration on image quality and quantification. The standard K_2HPO_4 density showed higher CT values than the actual bone CT values. Furthermore, we determined the optimal K_2HPO_4 density using CT values for the bone SPECT image evaluation.

The CT values obtained with the standard density exceeded 1,000 HU in the SPECT/CT system. The mean CT values for the vertebral bones range from 51.8 to 175.0 HU when stratified by age [15] and decreased significantly with age. The CT values in the present study were higher than those in previous studies, raising the possibility that bone SPECT phantom studies have been performed with a higher attenuation coefficient than that of actual bone. The K_2HPO_4 densities obtained CT values of 50–200 HU, which are close to those of vertebral bones (0.1–0.2 g/cm^3). In quantitative brain perfusion SPECT, several studies have reported that non-uniform attenuation maps, including the skull bone, are required to improve quantitative accuracy [16, 17]. The CT values corresponding to the vertebral bones should be reproduced when bone SPECT is evaluated using the SIM^2 bone phantom. Ichikawa et al. evaluated the effect of K_2HPO_4 solutions with different CT values and reported that high CT values caused the overcorrection of accumulation in a special image reconstruction method [9]. Furthermore, the bone density showed 106.52 ± 58.00 HU in ^{99m}Tc-diphosphonopropanedicarboxylic acid SPECT/CT imaging [18]. Based on our previous studies and our results, we determined an optimal K_2HPO_4 density of 0.15 g/cm^3.

The spatial resolution differs with and without a bone-equivalent solution when scattered radiation, attenuation, and spatial resolution corrections are performed in an experiment. Ito et al. reported differences in the image quality of the vertebral body, protrusion, and tumorous parts with and without a bone-equivalent solution [19]. Hashizume et al. reported that the measured radioactivity of a high-density K_2HPO_4 solution was higher than that of water (less than 5%) [20]. As a result, the point spread function in the spinous process is sharper than that of water, and it is possible that the FWHM decreased therein. Spatial resolution is a major parameter for image quality, and using a bone-equivalent solution may be necessary for evaluation using SIM^2 bone phantoms.

The %CVs of the background showed no significant difference. In this study, SIM^2 bone phantoms were repetition-created thrice to validate the impact of bone-equivalent

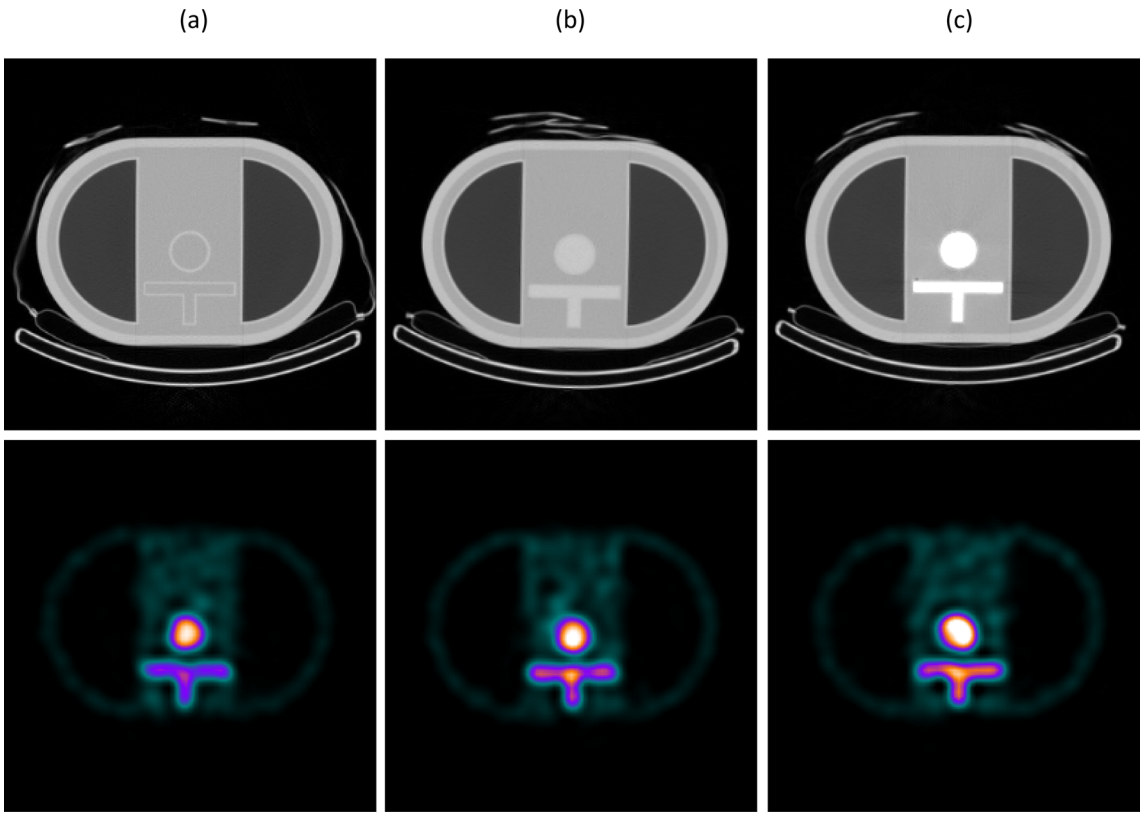

Fig. 8 CT (upper row) and SPECT (lower row) images. **a** Water used in the spine. **b** K_2HPO_4 with optimized density 0.15 g/cm^3. **c** K_2HPO_4 with a standard density 1.49 g/cm^3

solution density. In addition, compared to Fukami et al.'s [12] study using the SIM^2 bone phantom conducted under the same image reconstruction conditions, the differences in the background uniformity were slight, indicating the high reproducibility of the created phantom.

The recovery coefficients did not differ between the standard and optimized K_2HPO_4 densities. However, the recovery coefficient obtained using water was lower than that obtained using the bone-equivalent solution. This result is consistent with that of spatial resolution, and usage of a bone-equivalent solution allows a highly accurate assessment of lesion detectability in bone SPECT phantom studies.

The background SUV_{mean} did not differ significantly between the water alone and bone-equivalent solution. Okuda et al. validated the reproducibility of quantitative measurements with seven devices using a cylindrical phantom and reported a difference of approximately 4% [21]. In this study, SIM^2 bone phantom preparation and acquisition were performed at different time points. Nevertheless, the difference in the background SUV_{mean} was approximately 3%. In general, high objectivity and reproducibility are important for phantom evaluation. Although using a bone-equivalent solution increases the complexity of the control techniques, SIM^2 bone phantoms have good potential for multicenter evaluations involving several different SPECT/CT and positron emission tomography/CT devices.

The SUV_{mean} values of the spheres depend on the concentration of the bone-equivalent solution. This result can be explained in terms of the spatial resolution and recovery coefficient. An optimized bone-equivalent solution density is necessary as it affects the image quality and quantitative accuracy.

A limitation of this study is that we examined only one commercially available SPECT/CT device and applied limited imaging parameters. The HU values from CT data depend on the effective tube voltage [22, 23]. In addition, Onishi et al. reported that the optimal reconstruction parameters differ among the resolution recovery algorithms [24]. Therefore, further studies using several SPECT/CT scanners and different tube voltages are necessary.

5 Conclusions

We evaluated the effect of bone-equivalent solution concentration on SPECT image quality and quantification. It was found that image quality and quantification depends on the presence/absence and concentration of the bone-equivalent

solution. In bone-related phantom experiments, it is desirable to use a bone-equivalent solution adjusted to a concentration that yields the desired CT value.

Declarations

Conflict of interest The authors have no conflicts of interest to declare.

Ethical approval This article does not contain any studies performed on human participants or animals.

Informed consent There are no human subjects involved in this work.

References

1. Romer W, Nomayr A, Uder M, Bautz W, Torsten K. SPECT-guided CT for evaluating foci of increased bone metabolism classified as indeterminate on SPECT in cancer patients. J Nucl Med. 2006;47(7):1102–6.
2. Even-Sapir E, Metser U, Mishani E, Lievshitz G, Lerman H, Leibovitch I. The detection of bone metastases in patients with high-risk prostate cancer: 99mTc-MDP planar bone scintigraphy, single- and multi-field-of-view SPECT, ^{18}F-Fluoride PET, and ^{18}F-fluoride PET/CT. J Nucl Med. 2006;47(2):287–97.
3. Abikhzer G, Gourevich K, Kagna O, Israel O, Frenkel A, Keidar Z. Whole-body bone SPECT in breast cancer patients: the future bone scan protocol? Nucl Med Commun. 2016;37(3):247–53.
4. Kaneta T, Ogawa M, Daisaki H, Nawata S, Yoshida K, Inoue T. SUV measurement of normal vertebrae using SPECT/CT with Tc-99m methylene diphosphonate. Am J Nucl Med Mol Imaging. 2016;6(5):262–8.
5. Nakahara T, Daisaki H, Yamamoto Y, Iimori T, Miyagawa K, Okamoto T, et al. Use of a digital phantom developed by QIBA for harmonizing SUVs obtained from the state-of-the-art SPECT/CT systems: a multicenter study. EJNMMI Res. 2017;7(1):53. https://doi.org/10.1186/s13550-017-0300-5.
6. Hishikawa M, Matsutomo N, Yamamoto T. Impact of reconstruction parameters on quantitative bone SPECT imaging: a novel thoracic spine phantom study. Hell J Nucl Med. 2019;22:140.
7. Shibutani T, Onoguchi M, Naoi Y, Yoneyama H, Konishi T, Tatami R, et al. The usefulness of SwiftScan technology for bone scintigraphy using a novel anthropomorphic phantom. Sci Rep. 2021;11(1):2644. https://doi.org/10.1038/s41598-021-82082-x.
8. Ichikawa H, Kawakami K, Onoguchi M, Shibutani T, Nagatake K, Hosoya T, et al. Automatic quantification package (Hone Graph) for phantom-based image quality assessment in bone SPECT: computerized automatic classification of detectability. Ann Nucl Med. 2021;35(8):937–46. https://doi.org/10.1007/s12149-021-01631-6.
9. Ichikawa H, Miyaji N, Onoguchi M, Shibutani T, Nagaki A, Kato T, et al. Feasibility of ultra-high-speed acquisition in xSPECT bone algorithm: a phantom study with advanced bone SPECT-specific phantom. Ann Nucl Med. 2022;36(2):183–90. https://doi.org/10.1007/s12149-021-01689-2.
10. Ichikawa H, Kato T, Shimada H, Watanabe Y, Miwa K, Matsutomo N, et al. Detectability of thoracic bone scintigraphy evaluated using a novel custom-designed phantom. The Jpn J Nucl Med Technol. 2017;37(3):229–38.
11. de Dreuille O, Strijckmans V, Ameida P, Loc'h C, Bendriem B. Bone equivalent liquid solution to assess accuracy of transmission measurements in SPECT and PET. IEEE Trans Nucl Sci. 1997;44(3):1186–90.
12. Fukami M, Matsutomo N, Yamamoto T. Optimization of number of iterations as a reconstruction parameter in bone SPECT imaging using a novel thoracic spine phantom. J Nucl Med Technol. 2021;49(2):143–9. https://doi.org/10.2967/jnmt.120.253534.
13. Iida H, Hori Y, Ishida K, Imabayashi E, Matsuda H, Takahashi M, et al. Threedimensional brain phantom containing bone and grey matter structures with a realistic head contour. Ann Nucl Med. 2013;27(1):25–36. https://doi.org/10.1007/s12149-012-0655-7.
14. Gittoes N. Osteoporosis: pathophysiology and clinical management. Clin Endocrinol (Oxf). 2003;59(6):826–7. https://doi.org/10.1046/j.1365-2265.2003.01904.x.
15. Lee S, Chung CK, Oh SH, Park SB. Correlation between bone mineral density measured by dual-energy X-ray absorptiometry and Hounsfield units measured by diagnostic CT in lumbar spine. J Korean Neurosurg Soc. 2013;54(5):384–9. https://doi.org/10.3340/jkns.2013.54.5.384.
16. Ichihara T, Motomura N, Ogawa K, Hasegawa H, Hashimoto J, Kubo A. Evaluation of SPET quantification of simultaneous emission and transmission imaging of the brain using a multidetector SPET system with the TEW scatter compensation method and fan-beam collimation. Eur J Nucl Med. 1996;23(10):1292–9. https://doi.org/10.1007/BF01367583.
17. Licho R, Glick SJ, Xia W, Pan TS, Penney BC, King MA. Attenuation compensation in ^{99m}Tc SPECT brain imaging: a comparison of the use of attenuation maps derived from transmission versus emission data in normal scans. J Nucl Med. 1999;40(3):456–63.
18. Cachovan M, Vija AH, Hornegger J, Kuwert T. Quantification of ^{99m}Tc-DPD concentration in the lumbar spine with SPECT/CT. EJNMMI Res. 2013;3(1):1–8. https://doi.org/10.1186/2191-219X-3-45.
19. Ito T, Tsuchikame H, Ichikawa H, Onoguchi M, Okuda K, Shibutani T, et al. Verification of phantom accuracy using a Monte Carlo simulation: bone scintigraphy chest phantom. Radiol Phys Technol. 2021;14(3):336–44. https://doi.org/10.1007/s12194-021-00631-5.
20. Hashizume K, Ichikawa Y, Tomita Y, Sakuma H. Impact of CT tube-voltage and bone density on the quantitative assessment of tracer uptake in Tc-99m bone SPECT/CT: a phantom study. Phys Med. 2022;104:18–22. https://doi.org/10.1016/j.ejmp.2022.10.022.
21. Okuda K, Fujii S, Sakimoto S. Impact of novel incorporation of CT-based segment mapping into a conjugated gradient algorithm on bone SPECT imaging: fundamental characteristics of a context-specific reconstruction method. Asia Ocean J Nucl Med Biol. 2019;7(1):49–57. https://doi.org/10.22038/AOJNMB.2018.31711.1219.
22. Rappoport V, Carney JP, Townsend DW. CT tube-voltage dependent attenuation correction scheme for PET/CT scanners. IEEE Symp Conf Rec Nucl Sci. 2004;2004(6):3853–7. https://doi.org/10.1109/NSSMIC.2004.1466720.
23. Bornefalk H. Synthetic hounsfield units from spectral CT data. Phys Med Biol. 2012;57(7):83–7. https://doi.org/10.1088/0031-9155/57/7/N83.
24. Onishi H, Motomura N, Fujino K, Natsume T, Haramoto Y. Quantitative performance of advanced resolution recovery strategies on SPECT images: evaluation with use of digital phantom models. Radiol Phys Technol. 2013;6(1):42–53. https://doi.org/10.1007/s12194-012-0168-z.